Journal of The Electrochemical Society, **157** (6) K131-K137 (2010)
0013-4651/2010/157(6)/K131/7/$28.00 © The Electrochemical Society

Interaction Between Carbonaceous Structure and Functionalized Single-Walled Carbon Nanotubes

Jung-Ah Lee,[a,b] Byung Chul Lee,[a] Sang-Myung Lee,[a] Kyeong-Kap Paek,[c] Byeong-Kwon Ju,[d] Yun-Hi Lee,[b] and Hyun Joon Shin[a,z]

[a]*Nano-Bio Photonics Laboratory, Nano-Bio Research Center, Korea Institute of Science and Technology, Seongbuk-gu, Seoul 136-791, Republic of Korea*
[b]*Department of Physics and* [d]*School of Electrical Engineering, Korea University, Seongbuk-gu, Seoul 136-713, Republic of Korea*
[c]*Department of Electronic Engineering, Daejin University, Pocheon, Gyeonggi-do 487-711, Republic of Korea*

The properties of functionalized single-walled carbon nanotube (f-SWCNT) supernatant samples obtained through steps of acid oxidation–centrifugation–decantation were characterized by spectroscopic tools. Fourier transform IR spectroscopy provided evidence for the chemical and structural variations generated on the f-SWCNTs within each supernatant sample. The results from UV-visible near-IR spectroscopy revealed that the density difference of the carbonaceous impurity with functional groups on the f-SWCNTs contributed to the attenuation of electrical conductivity. In the Raman results, the shift of frequency in the radial breathing mode (RBM) was associated with an increase in diameter of the f-SWCNTs and a decrease in RBM intensity was attributed to the depletion of valence band electrons. The redshift of the tangential mode indicates the reduction in the bandgaps of the f-SWCNTs by the decrease in carbonaceous impurity.
 [DOI: 10.1149/1.3355946]

Manuscript submitted October 13, 2009; revised manuscript received February 9, 2010. Published April 27, 2010.

Single-walled carbon nanotubes (SWCNTs) have been perceived as an attractive material due to their excellent electrical, thermal, and mechanical properties. Recently, research on SWCNTs has been carried out in various fields from basic research to industrial applications.[1,2] For example, SWCNTs have been used as reinforcing elements for composite materials.[3,4] Some researchers have devoted their attention to developing green technology such as solar cell and hydrogen and energy storages using SWCNTs as raw materials.[5-12] The transport studies of SWCNTs have been attempted for nanosized electronic systems.[13-16] In addition to the above research issues, the research field for potential applications of SWCNTs includes gas and flow sensors, electromechanical devices, and nanobiosensors.[17-22] However, despite this extensive research, several technical hurdles such as high cost, selectively separating the nanotubes, solubility, difficulties in assembly, etc., still remain. To overcome these barriers, effective methods have also been suggested by many credible researchers.[23-28]

Among these effective methods, the oxidation of carbon nanotubes by strong acids and other oxidizing agents is regarded as a basic condition for the realization of vast potential applications and is treated as an important issue in the area of physical and chemical properties of carbon nanotubes (CNTs). Through the oxidation process by strong acids, the CNTs have experienced changes in length, defect generation, and so on. In addition, the CNTs are functionalized by a high density of oxygen-containing groups, mainly carboxyl (COOH) groups. These oxidation products formed in the oxidation process not only affect the structural stabilities and electronic properties of functionalized CNTs but can also determine the main properties of their potential applications.[29-33] For instance, the experimental results measured by Shao et al. showed that the oxidation product called oxidation debris acts as a shielding material for the nanotube walls. In addition, Shao's group mentioned that its removal should be considered before doing any chemical treatment.[31] Therefore, this paper tries to verify the interaction between oxidized SWCNTs and oxidation products for applications of oxidized SWCNTs as nanosized building blocks with a specific functional group. The samples for measurement were prepared in three steps and were characterized by optical spectroscopies. The results show that the presence of the oxidation product is a significant parameter in the electronic structures of oxidized SWCNTs.

[z] E-mail: kaiphy@kist.re.kr

Experimental

The SWCNTs produced by the arc-discharge method (ILJIN Nanotec. Co. Ltd., Korea) were used for the experiments, and their mean diameter and length were estimated to be 1.4 nm and 5–20 μm, respectively. The dispersion of SWCNTs was accomplished by a mixture of two strong acids. The SWCNTs (10 mg) were suspended in 40 mL of a mixture of nitric and sulfuric acids with a volume ratio of 1:3.[34,35] The mixture was stirred for 48 h at room temperature and sonicated for 10 h using a Branson water bath sonicator (40 kHz, 185 W). This reaction mixture was diluted with 200 mL of distilled water. The diluted solution was filtered through a 0.2 μm pore size Millipore filter membrane under vacuum with an aspirator. The residue formed on the filter membrane was repeatedly washed using 10 mM NaOH solution and distilled water until the pH of the filtrates was 7. The residue mat was immersed in distilled water and sonicated for 30 min to separate the mat from the filter. Subsequently, stirring was continued for 30 min at room temperature. As a result, a stable and homogeneous SWCNT suspension was obtained.

The centrifugal process was applied to separate the elements of the SWCNT suspension. The prepared SWCNT suspension was distributed into 1.5 mL microcentrifuge tubes for centrifugation. The microcentrifuge tubes were centrifuged at 15,000 rpm for 10 h at 4 °C. The supernatants formed in the microcentrifuge tubes were extracted using two decanting methods and were collected into the sample bottles. The decanting methods were denoted as method A and method B. The samples prepared by the decanting methods A and B were denoted as group I and group II, respectively. After the removal of the supernatant, the sediments were resuspended in deionized water and the centrifugal process was again carried out. The experimental process developed as the dispersion–centrifugation–decantation cycle was repeated four times at 90 min intervals (Fig. 1 and Table I).

The characterization of each sample was developed using a Fourier transform infrared spectroscope (FTIR, Thermo Nicolet 6700, Nicolet Almega FTIR spectrometer), an ultraviolet-visible near-infrared (UV-VIS-NIR) spectroscope (Varian Cary 5000 spectrophotometer), and a Raman spectroscope with an excitation wavelength of 532 nm and 25 mW laser power (Thermo Nicolet, Almega XR, dispersive Raman spectrometer).

Results and Discussion

FTIR.— The FTIR measurements were carried out to understand both the chemical and the IR vibrational features of the acid-treated

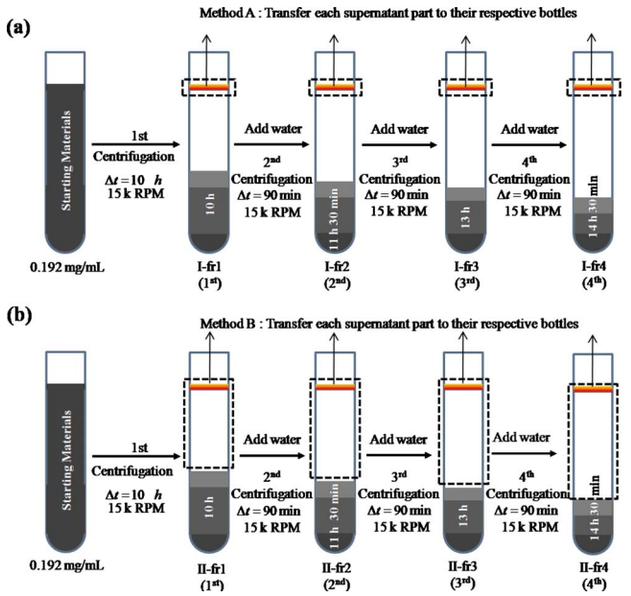

Figure 1. (Color online) Schematic of the dispersion–centrifugation–decantation cycles containing two extraction methods used in the decantation step. (a) Method A and (b) method B.

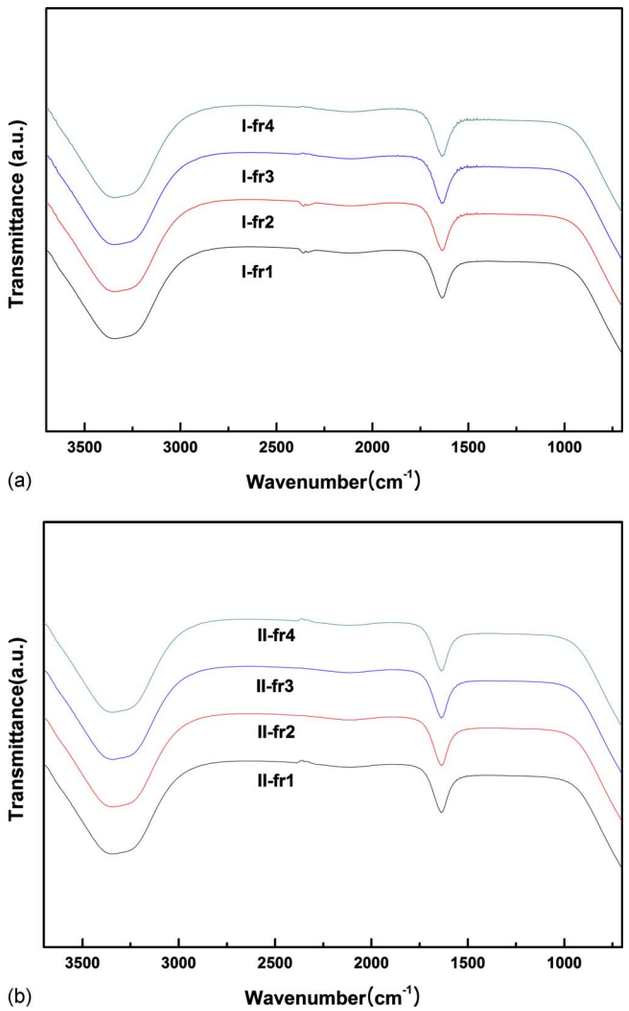

Figure 2. (Color online) The FTIR results of oxidized SWCNT supernatant samples. (a) Method A and (b) method B.

SWCNTs contained in the samples produced by methods A and B. The FTIR spectra of each sample are shown in Fig. 2a and b. These results did not indicate any obvious difference from the comparisons drawn between group I and group II.

The main characteristics of the FTIR absorption bands were observed around 1500–1750 and 3000–3500 cm^{-1}. For convenience, the former is denoted as IR-a and the latter is denoted as IR-b. IR-a with a peak at 1630 cm^{-1} as a point of inflection displays an asymmetric shape. The asymmetric profile of the band at 1630 cm^{-1} reveals the presence of anionic carboxylates and this peak was also assigned to the C═O stretching mode of carbonylic moiety.[36] Typically, the peak at 1630 cm^{-1} is detected as a very weak signal in perfect SWCNTs because of the symmetry of the dipole moment.[37-39] Furthermore, this peak corresponded to the C═C stretching mode of SWCNT graphitic layers near the modified sites, which is IR-activated by extensive sidewall functionalization.[38,40,41] From these facts, it is evident that the peak at 1630 cm^{-1} existed by the functionalization of SWCNTs.

The SWCNTs used in this paper were oxidized by the nitric and sulfuric acid mixture. Through the oxidation, the surface of SWCNTs was covered with the oxidation impurity such as carboxylic defects, small carbonaceous impurity.[42-44] With regard to the aspects of electrical properties of SWCNTs, the oxidized SWCNTs obtained by the nitric and sulfuric acids are dominated with hole carriers.[42-48] These changes mentioned until now originated from the functionalization. Considering together the chemical and electrical changes, the peak at 1630 cm^{-1} can be regarded as a feature of

Table I. Centrifugal conditions for obtaining the samples used in the experiments.

			Method A		
Samples	I-fr1	I-fr2	I-fr3	I-fr4	
Centrifugal condition	15 k rpm, 10 h	15 k rpm, 11 h 30 min	15 k rpm, 13 h	15 k rpm, 14 h 30 min	0.192 mg/mL SWCNT solution
Sample pickup	From the top of the solution	From the top of the solution	From the top of the solution	From the top of the solution	Starting material
			Method B		
Samples	II-fr1	II-fr2	II-fr3	II-fr4	
Centrifugal condition	15 k rpm, 10 h	15 k rpm, 11 h 30 min	15 k rpm, 13 h	15 k rpm, 14 h 30 min	0.192 mg/mL SWCNT solution
Sample pickup	Without the precipitation of the solution	Without the precipitation of the solution	Without the precipitation of the solution	Without the precipitation of the solution	Starting material

carboxylic defects and hole carriers existing on the graphitic layer of functionalized single-walled carbon nanotubes (f-SWCNTs) in each sample.

In the second band denoted as IR-b, the absorption spectra were measured as an asymmetric broad band. This asymmetric broad band is estimated to be due to the presence of water within the samples.[49] The stretching mode of the –OH group of water is observed with a strong broad band at 3400 cm^{-1}. The other possible reason is related to the –COOH group. This substituent in water reveals the asymmetric band of the –OH stretching mode of the –COOH group at 3400 cm^{-1}. Finally, on the basis of FTIR results, it can be concluded that the carboxyl-terminated SWCNTs are presented together with the feature of carboxylic defects and carboxylated carbonaceous impurity.

UV-VIS-NIR spectra.— The UV-VIS-NIR spectroscopy was attempted to know the variation in the composition of the pristine arc-discharge SWCNTs generated after the acid treatment. This optical measurement was also done to observe the modification in the electronic structure of f-SWCNTs in each sample. The absorption spectra from sample groups I and II are depicted in Fig. 3a and b, and Fig. 3c and d, respectively.[2,39,50-54]

Generally, the UV-VIS-NIR absorption spectrum of the arc-discharge SWCNTs consists of four bands. These four absorption bands are divided into a π-plasmon (200–300 nm), the first metallic interband transition ($M_{11} \approx$ 590–765 nm), and the first ($S_{11} \approx$ 1240–2100 nm) and the second ($S_{22} \approx$ 760–1250 nm) semiconducting interband transitions.[54] In contrast, the optical absorption spectra (Fig. 3a and c) are made up of three bands. The reason is that the M_{11} interband transition disappeared because of the selective reactivity between metallic SWCNTs and mixed acids, as described in the associated paper.[34,35]

Based on the absorption properties of arc-discharge SWCNTs, the S_{11} and S_{22} interband transitions (Fig. 3a) are shifted to the right relative to those of the arc-discharge SWCNTs. The S_{11} interband transition is shifted from 1240–2100 to 1350–1600 nm, and the S_{22} interband transition is shifted from 760–1250 to 800–1350 nm. These results are due to the modulation in the electronic structure of the pristine arc-discharge SWCNTs after the oxidation reaction by acid treatment.

Figure 3b shows the enlarged image of the π-plasmon region depicted in Fig. 3a. This result reveals that the absorption intensity of each sample was reduced by repeating the experiments. The origin of the peaks located at 200–300 nm (Fig. 3b) is attributed to carbonaceous impurities such as small graphite particles, vacancy, and carboxyl group. The position of these peaks is defined as the π-plasmon frequency of carbonaceous impurities.[55]

Meanwhile, the background under these peaks is associated with the π-plasmon oscillation between carbonaceous impurities and SWCNTs.[56] The interaction of these materials was estimated to form the high energy absorption background.[56] Moreover, the important point is that the large proportion of the high energy absorption background of these peaks depends on the carbonaceous impurities.[56,57] Accordingly, the results of Fig. 3b proves that the profile changes of the π-plasmon peak were caused by the decrease in interaction between carbonaceous impurities and the defective SWCNTs.

As with the results of group II (Fig. 3c and d), the absorption spectra of the π-plasmon displayed an inclination which is not exactly separated into other curves. Therefore, this result implies that method B for preparing group II is less effective than method A.

Figure 4 shows the absorption spectra normalized to the values of the absorption at individual π-plasmon peaks, based on the optical spectra illustrated in Fig. 3.[58] The source of the π-plasmon peak is mostly carbonaceous impurities.[56,57] The purpose of normalization of the π-plasmon peak is to investigate the electronic interband transitions of the f-SWCNTs that arise due to the carbonaceous impurity.

After the individual normalization of each sample, the obtained absorption spectra were divided into two parts of the S_{11} and S_{22}

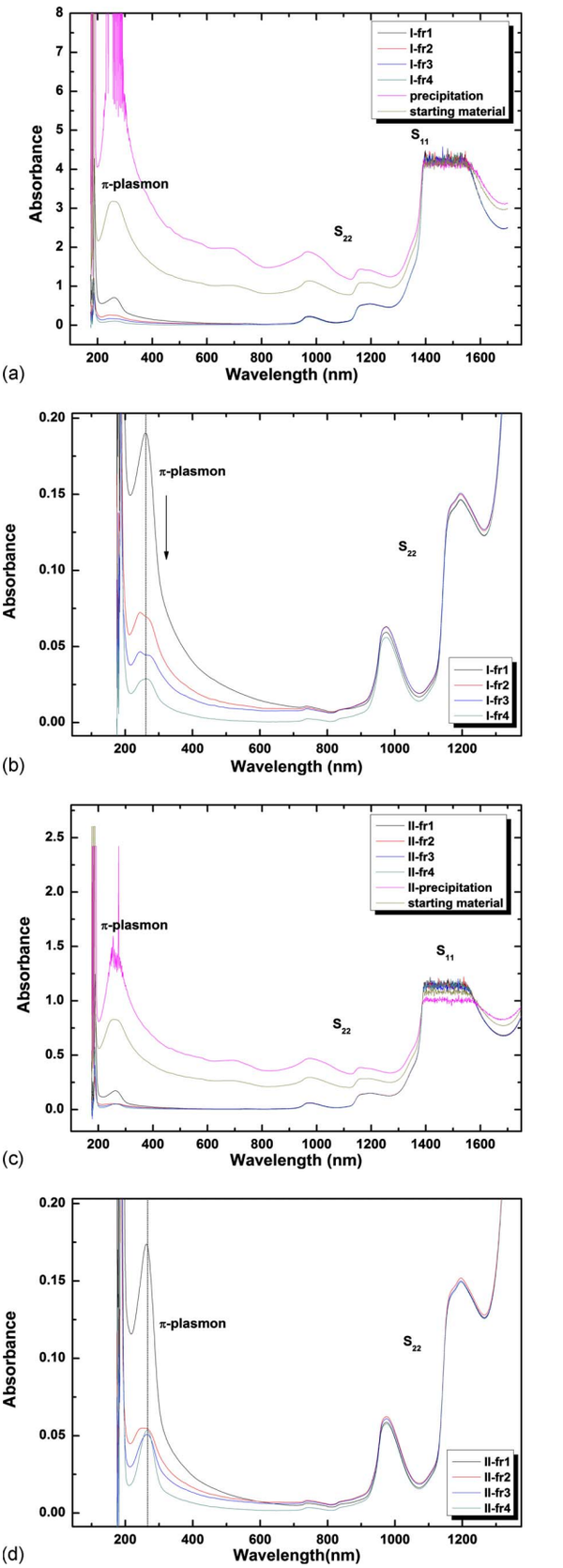

Figure 3. (Color online) The UV-VIS-NIR absorption spectra of oxidized SWCNT supernatant samples. (a) and (b): Method A; (c) and (d): method B.

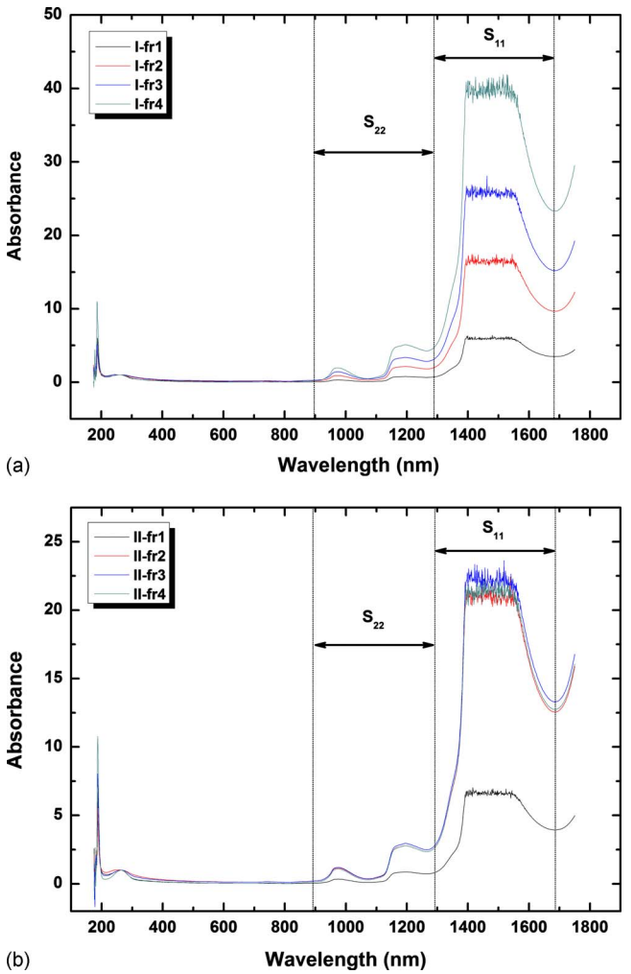

Figure 4. (Color online) The UV-VIS-NIR absorption spectra obtained from the oxidized SWCNT supernatant samples. (a) Method A and (b) method B.

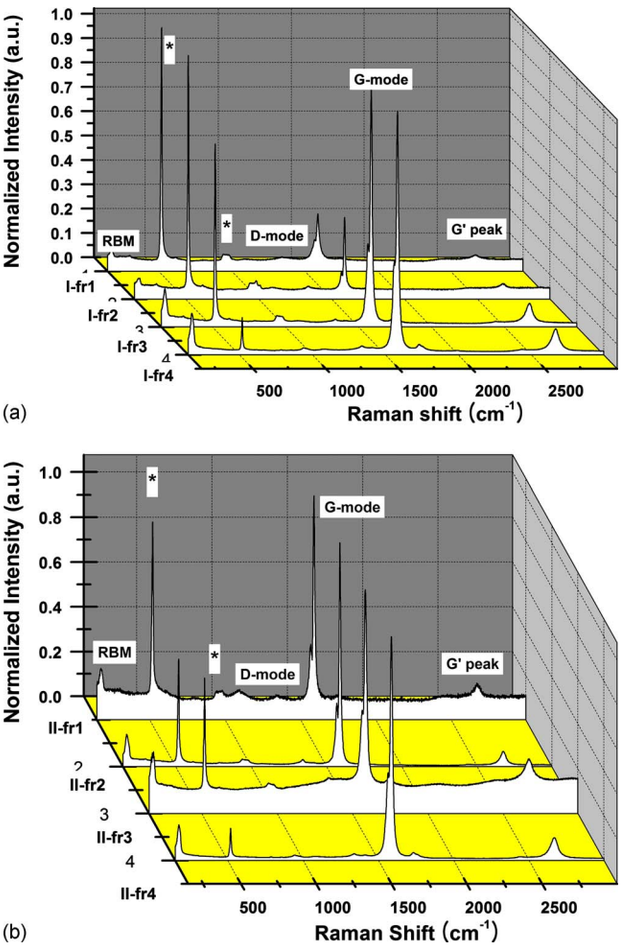

Figure 5. (Color online) The Raman spectra of the oxidized SWCNT supernatant samples. (a) Method A and (b) method B.

electronic interband transitions. Some wavelength regions of these absorption spectra appeared as a flat horizontal line. This result is related to carbonaceous impurities. The presence of carboxylated carbonaceous impurities was confirmed by the FTIR results. The FTIR results revealed that each supernatant sample contained various carbon structures, such as C═O, COOH, C–OH moieties, and f-SWCNTs. The reason for the correlation between the flat spectra and carbonaceous impurities is that the absorption spectra of the oxidation derivatives consisting of high order carbon structures appeared as flat absorption spectra. This view is supported by the results from other groups studying the absorption spectra of the oxidation derivatives comprised of high order carbon structures.[39,59,60]

The first absorption band located in the wavelength range of 800–1350 nm was assigned to the second transition (S_{22}) between van Hove singularities (vHSs) of semiconducting single-walled carbon nanotubes (s-SWCNTs). This S_{22} interband transition was used mainly for the purity evaluation in the UV-VIS-NIR analysis of SWCNTs. The purity evaluation was achieved through the method proposed by Itkis et al. as a common method.[2] In Fig. 4a, the optical spectra of the S_{22} transition display an increasing behavior in the form of separate curves. This result indicates that the purity of each sample is enhanced along with the repetition of experiments.

The second absorption band (1350–1600 nm) was assigned to the first transition (S_{11}) between the vHSs of s-SWCNTs. The absorption intensity of S_{11} transitions shows an increasing trend. This behavior is assumed to be due to a variation in the number of charge carriers, which can cause changes in the electronic structure of f-SWCNTs within each sample. The reason is that the electronic structure of SWCNTs can be monitored by the S_{11} transition.

For the interpretation of results obtained from S_{11} and S_{22} transitions, other research papers were reviewed. Wang and colleagues described that the electrical conductivity of oxidized SWCNTs can be enhanced when the density of vacancy-carboxyl pairs (VCPs) on the surface of oxidized SWCNTs is increased.[61] The term "VCPs" used in Wang et al.'s paper can be included in the meaning of the carbonaceous impurity. This implies that the carbonaceous impurity such as VCPs in s-SWCNTs is associated with the electrical conductivity as charge carriers. According to Pekker et al.[62] and Geng et al.,[63] the intensity of S_{11} decreased during functionalization. This implies that the intensity of S_{11} is inversely proportional to the amount of carbonaceous impurity yield in the functionalization process.

From the above results, the increase in intensity in S_{11} absorption with the increase in S_{22} absorption clearly indicates the attenuation of electrical conductivity. This is consistent with the views expressed by Shim and Siddons.[64] Takenobu's group, who explained the carrier accumulation and optical property, supports the relevance of our experimental results.[65]

Raman spectra: RBM.— The Raman spectra of each sample, measured in the range of 150–3000 cm^{-1} using the laser excitation source of 532 nm, are presented in Fig. 5a and b. Peaks labeled with an asterisk (*) come from the Si/SiO_2 substrate (Fig. 5). As one of

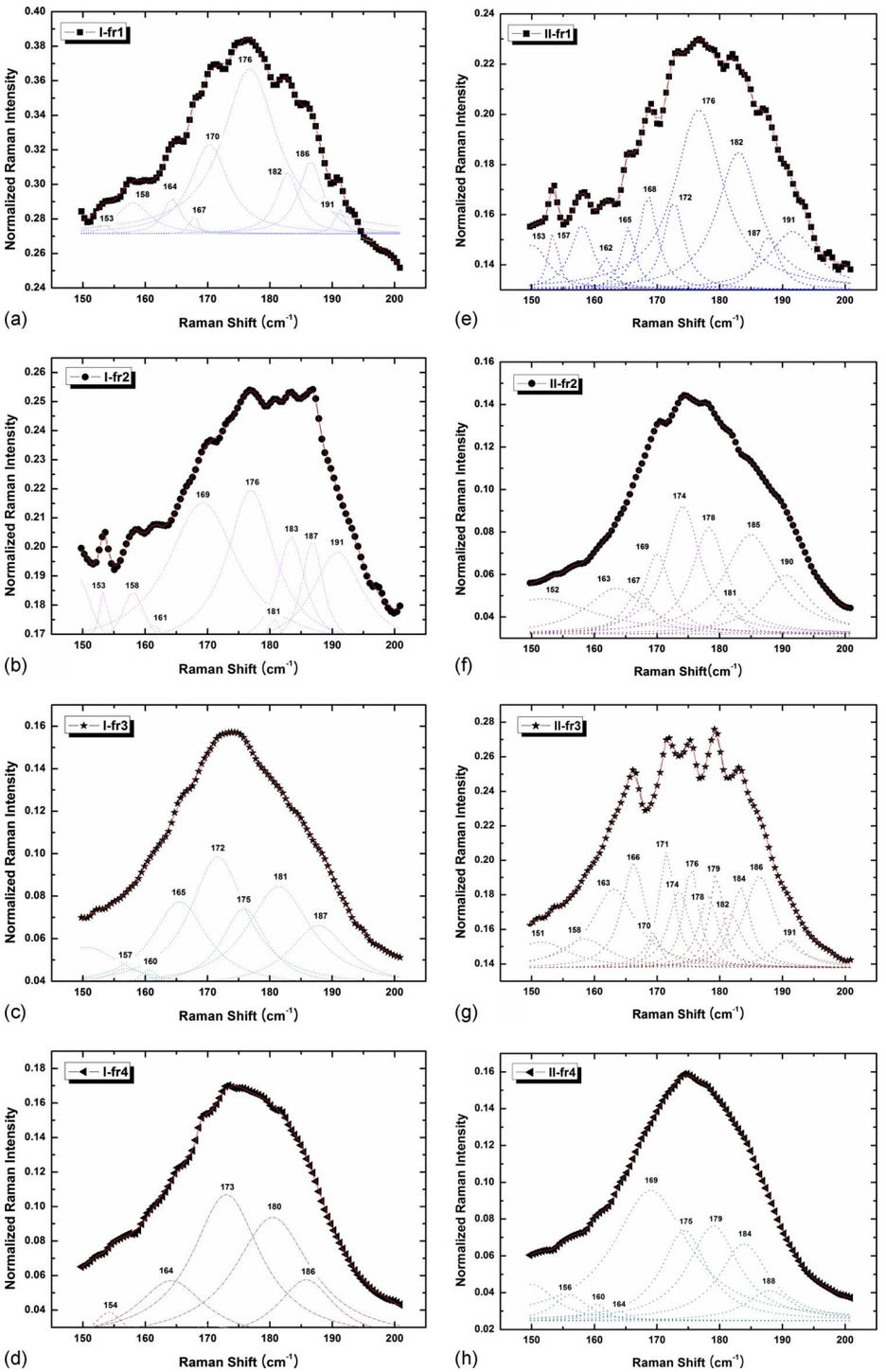

Figure 6. (Color online) The RBM spectra of the oxidized SWCNT supernatant samples. (a)-(d): Method A; (e)-(h): Method B.

the features of the Raman spectra (Fig. 5), the radial breathing mode (RBM) region is illustrated in Fig. 6a-h. The RBM frequencies in these figures were determined by the Lorentzian fitting method.

After the Lorentzian fit, the Lorentzian-fitted frequencies in Fig. 6a-d shifted to lower frequencies on the basis of the main peaks. This indicates that the diameter of f-SWCNTs increases gradually. The reason is that the characterization of the diameter distribution for the f-SWCNTs is determined with the relation $\omega_{RBM} = (A/d_t) + B$, where ω_{RBM} is the RBM frequency shift in cm^{-1}, with d_t the tube diameter in nanometers. The values of constants A and B are empirically determined, and the reported values for A and B are 224–248 cm^{-1} nm and 8–14 cm^{-1}, respectively.[66-74] Especially, constant B is a scaling constant for intertube interaction, which depends on the bundle diameter.[75-77] The results in Fig. 6a-d, showing an increase in diameter of f-SWCNTs, are consistent with the experimental result in Ref. 34. In contrast, the results in Fig. 6e-h do not show the consistency in the RBM frequencies (group II by method B).

The peak shift in Fig. 6a-d also indicates that the movements are attributed to the change in the resonance condition by the partial

removal of the carbonaceous impurities in each sample. In conclusion, the results in Fig. 6a-d indicate that the electronic structure of f-SWCNTs in each sample is changed by the removal of carbonaceous impurities.

Next, the RBM intensities (Fig. 6a-d) have shown a decreasing trend. However, it is difficult to find appropriate features from the RBM intensities shown in Fig. 6e-h. The Raman signal intensity is associated with the laser photon energy (E_L), the optical transition energy (E_{ii}), and the phonon energy (E_{ph}).[78] The optical transition energy E_{ii} presents the energy separation between the ith vHSs, and this value is inversely proportional to the tube diameter.[79]

It is already confirmed from the shift of RBM frequency that the diameter of f-SWCNTs increased from I-fr1 to I-fr4. If this result is applied to the optical transition energy E_{ii}, it can be concluded that the energy separation E_{ii} of f-SWCNTs within each sample decreased.

In addition, the RBM intensity can be determined by the depletion or filling of the nanotube electronic bands due to chemical doping.[80]

According to the paper of Wang's group, bandgap E_{ii} is proportional to the density of VCPs.[61] The samples mentioned in this paper were prepared by a centrifugation step for the purpose of controlling the amount of carbonaceous impurities in each sample. It is confirmed that the amount of carbonaceous impurities decreased after the centrifugation, which implies the decrease in both the density of VCPs and energy separation E_{ii}. The attenuation of energy separation E_{ii} presents the loss of resonance enhancement between the ith vHSs because the Raman spectra of SWCNTs are resonance-enhanced via the optical transition between vHSs.[79] This behavior, which is related to the optical transition energy, occurred when the electrons in valence band singularities were depleted.[80] Therefore, it is concluded that the decrease in the intensity of RBM profiles is attributed to the depletion of valence band electrons in the electronic structure of f-SWCNTs contained in each sample.

Tangential mode.— Figure 7 shows the Raman spectra of the tangential mode (G band) obtained for each sample.[81-83] The G band spectra in Fig. 7a moved toward low frequencies, and this shift corresponds with the redshift. In Fig. 7b, the tangential modes did not show the shift. The result in Fig. 7a appeared as the redshift of the G band and can be regarded as evidence of the reduction of the f-SWCNTs energy gap by the equation $E = hc/\lambda$. To elucidate the reason for the variation in the energy gap, the comparison of relative intensity ratios between D, G, and G′ bands were introduced.[82] The comparison of relative intensity changes in the D and G bands (I_D/I_G) of the Raman results is plotted on the left side of Fig. 7c. The intensity ratio in the D and G′ bands ($I_D/I_{G'}$) is plotted on the right side of Fig. 7c.[30,82] The ratios of I_D/I_G and $I_D/I_{G'}$ decreased only in group I. This implies that the carbonaceous impurity in group I was gradually reduced by the repetition of decantation. These behaviors of I_D/I_G and $I_D/I_{G'}$ conform to the decrease in the density of VCP's treated in Wang et al.'s paper.[61] Therefore, from the redshift in the G band and the changes in relative intensity ratios, it is possible to presume that the reduction of the energy bandgap was affected by the decrease in carbonaceous impurity. This relationship, with respect to the results obtained from Fig. 7, is supported by Wang et al.'s result that the upward shift of the defect band is achieved by the decrease in the density of VCPs.[61] Accordingly, the interpretation of our results and Wang et al.'s results is derived from the conclusion that the redshift observed in the tangential mode indicates the reduction in the bandgaps of f-SWCNTs by the decrease in carbonaceous impurity.

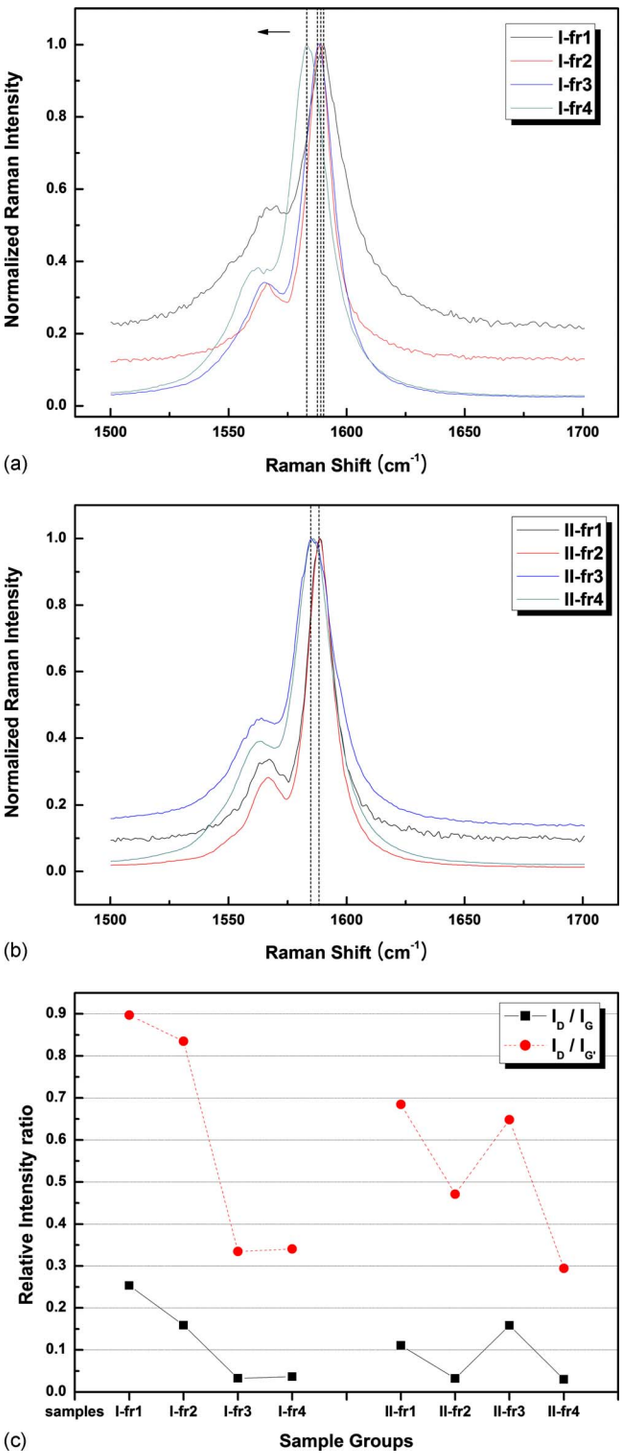

Figure 7. (Color online) The G band Raman spectra of oxidized SWCNT supernatant samples. (a) Method A, (b) method B, and (c) relative intensity ratio of I_D/I_G and $I_D/I_{G'}$.

Conclusions

This study provides insight into the relationship between f-SWCNTs and the carbonaceous impurity generated in the functionalization process. The characteristics of f-SWCNTs coexisting with the carbonaceous impurity have been evaluated by FTIR, UV-VIS-NIR, and Raman spectroscopy. The FTIR data show evidence of chemical and structural variations generated on the f-SWCNTs within each supernatant sample. The UV-VIS-NIR results indicate that an increased absorption at the transition between the first pairs of vHSs is related to the decrease in the electrical conductivity. The results obtained from Raman measurement verified that the carbonaceous impurity is a material associated with the control of the

bandgap. Our results demonstrate that a quantitative control of carbonaceous impurity after acid oxidation is needed for various applications of f-SWCNTs.

Acknowledgments

This research was supported by KIST Basic R&D Projects sponsored by the Korea Institute of Science and Technology. The authors acknowledge the continuing help of Dr. Sang-Woo Kim and Dr. Kyung Yoon Chung at KIST. J.-A.L. acknowledges the support of the Seoul Science Fellowship program of the Seoul Metropolitan Government.

Korea Institute of Science and Technology assisted in meeting the publication costs of this article.

References

1. F. Simon, M. Galambos, D. Quintavalle, B. Náfrádi, L. Forró, J. Koltai, V. Zólyomi, J. Kürti, N. M. Nemes, M. H. Rümmeli, et al., *Phys. Status Solidi B*, **245**, 1975 (2008).
2. M. E. Itkis, D. E. Perea, S. Niyogi, S. M. Rickard, M. A. Hamon, H. Hu, B. Zhao, and R. C. Haddon, *Nano Lett.*, **3**, 309 (2003).
3. V. P. Veedu, A. Cao, X. Li, K. Ma, C. Soldano, S. Kar, P. M. Ajayan, and M. N. Ghasemi-nejhad, *Nature Mater.*, **5**, 457 (2006).
4. A. A. Mamedov, N. A. Kotov, M. Prato, D. M. Guldi, J. P. Wicksted, and A. Hirsch, *Nature Mater.*, **1**, 190 (2002).
5. J. U. Lee, *Appl. Phys. Lett.*, **87**, 073101 (2005).
6. Z. Li, V. P. Kunets, V. Saini, Y. Xu, E. Dervishi, G. J. Salamo, A. R. Biris, and A. S. Biris, *Appl. Phys. Lett.*, **93**, 243117 (2008).
7. A. C. Dillon, K. M. Jones, T. A. Bekkedahl, C. H. Kiang, D. S. Bethune, and M. J. Heben, *Nature (London)*, **386**, 377 (1997).
8. C. Liu, Y. Y. Fan, M. Liu, H. T. Cong, H. M. Cheng, and M. S. Dresselhaus, *Science*, **286**, 1127 (1999).
9. D. M. Guldi, G. M. Rahman, M. Prato, N. Jux, S. Qin, and W. Ford, *Angew. Chem., Int. Ed.*, **44**, 2015 (2005).
10. C. Niu, E. K. Sichel, R. Hoch, D. Moy, and H. Tennent, *Appl. Phys. Lett.*, **70**, 1480 (1997).
11. E. Frackowiak and F. Béguin, *Carbon*, **40**, 1775 (2002).
12. K. H. An, W. S. Kim, Y. S. Park, Y. C. Choi, S. M. Lee, D. C. Chung, D. J. Bae, S. C. Lim, and Y. H. Lee, *Adv. Mater.*, **13**, 497 (2001).
13. C. T. White and T. N. Todorov, *Nature (London)*, **393**, 240 (1998).
14. S. U. Choi, Z. G. Zhang, W. Yu, F. E. Lockwood, and E. A. Grulke, *Appl. Phys. Lett.*, **79**, 2252 (2001).
15. M. J. Biercuk, M. C. Llaguno, M. Radosavljevic, J. K. Hyun, A. T. Johnson, and J. E. Fischer, *Appl. Phys. Lett.*, **80**, 2767 (2002).
16. J. K. Holt, H. G. Park, Y. Wang, M. Stadermann, A. B. Artyukhin, C. P. Grigoropoulos, A. Noy, and O. Bakajin, *Science*, **312**, 1034 (2006).
17. J. Li, Y. Lu, Q. Ye, M. Cinke, J. Han, and M. Meyyappan, *Nano Lett.*, **3**, 929 (2003).
18. S. Ghosh, A. K. Sood, and N. Kumar, *Science*, **299**, 1042 (2003).
19. R. H. Baughman, C. Cui, A. A. Zakhidov, Z. Iqbal, J. N. Barisci, G. M. Spinks, G. G. Wallace, A. Mazzoldi, D. D. Rossi, A. G. Rinzler, et al., *Science*, **284**, 1340 (1999).
20. V. Sazonova, Y. Yaish, H. Üstünel, D. Roundy, T. A. Arias, and P. L. McEuen, *Nature (London)*, **431**, 284 (2004).
21. N. Sinha, J. Ma, and J. T. Yeow, *J. Nanosci. Nanotechnol.*, **6**, 573 (2006).
22. B. L. Allen, P. D. Kichambare, and A. Star, *Adv. Mater.*, **19**, 1439 (2007).
23. K. Hata, D. N. Futaba, K. Mizuno, T. Namai, M. Yumura, and S. Iijima, *Science*, **306**, 1362 (2004).
24. A. G. Rinzler, *Nat. Nanotechnol.*, **1**, 17 (2006).
25. Z. Ren, *Nat. Nanotechnol.*, **2**, 17 (2007).
26. Y. Yao, Q. Li, J. Zhang, R. Liu, L. Jiao, Y. T. Zhu, and Z. Liu, *Nature Mater.*, **6**, 283 (2007).
27. Y. Huang, X. Duan, Q. Wei, and C. M. Lieber, *Science*, **291**, 630 (2001).
28. S. G. Rao, L. Huang, W. Setyawan, and S. Hong, *Nature (London)*, **425**, 36 (2003).
29. E. B. Barros, A. G. Filho, V. Lemos, J. M. Filho, S. B. Fagan, M. H. Herbst, J. M. Rosolen, C. A. Luengo, and J. G. Huber, *Carbon*, **43**, 2495 (2005).
30. C. G. Salzmann, S. A. Llewellyn, G. Tobias, M. A. Ward, Y. Huh, and M. L. Green, *Adv. Mater.*, **19**, 883 (2007).
31. L. Shao, G. Tobias, C. G. Salzmann, B. Ballesteros, S. Y. Hong, A. Crossley, B. G. Davis, and M. L. Green, *Chem. Commun. (Cambridge)*, **2007**, 5090.
32. A. López-Bezanilla, F. Triozon, S. Latil, X. Blase, and S. Roche, *Nano Lett.*, **9**, 940 (2009).
33. L. Li and R. J. Nicholas, *Nanotechnology*, **15**, 1844 (2004).
34. C. Yang, J. S. Park, K. H. An, S. C. Lim, K. Seo, B. Kim, K. A. Park, S. Han, C. Y. Park, and Y. H. Lee, *J. Phys. Chem. B*, **109**, 19242 (2005).
35. K. H. An, C. Yang, J. Y. Lee, S. C. Lim, C. Kang, J. Son, M. S. Jeong, and Y. H. Lee, *J. Electron. Mater.*, **35**, 235 (2006).
36. A. Arrais, E. Diana, D. Pezzini, R. Rossetti, and E. Boccaleri, *Carbon*, **44**, 587 (2006).
37. Y. Wang, Z. Iqubal, and S. Mitra, *J. Am. Chem. Soc.*, **128**, 95 (2006).
38. H. Yu, Y. Jin, Z. Li, F. Peng, and H. Wang, *J. Solid State Chem.*, **181**, 432 (2008).
39. A. Arrais, E. Boccaleri, and E. Diana, *Fullerenes, Nanotubes, Carbon Nanostruct.*, **12**, 789 (2004).
40. D. B. Mawhinney, V. Naumenko, A. Kuznetsova, J. T. Yates, Jr., J. Liu, and R. E. Smalley, *J. Am. Chem. Soc.*, **122**, 2383 (2000).
41. P. E. Fanning and M. A. Vannice, *Carbon*, **31**, 721 (1993).
42. A. Chou, T. Böcking, R. Liu, N. K. Singh, G. Moran, and J. J. Gooding, *J. Phys. Chem. C*, **112**, 14131 (2008).
43. G. U. Sumanasekera, J. L. Allen, S. L. Fang, A. L. Loper, A. M. Rao, and P. C. Eklund, *J. Phys. Chem. B*, **103**, 4292 (1999).
44. F. Hennrich, R. Wellmann, S. Malik, S. Lebedkin, and M. M. Kappes, *Phys. Chem. Chem. Phys.*, **5**, 178 (2003).
45. H. Tantang, J. Y. Ong, C. L. Loh, X. Dong, P. Chen, Y. Chen, X. Hu, L. P. Tan, and L. Li, *Carbon*, **47**, 1867 (2009).
46. W. Zhou, J. Vavro, N. M. Nemes, J. E. Fischer, F. Borondics, K. Kamarás, and D. B. Tanner, *Phys. Rev. B*, **71**, 205423 (2005).
47. Z. Wu, Z. Chen, X. Du, J. M. Logan, J. Sippel, M. Nikolou, K. Kamaras, J. R. Reynolds, D. B. Tanner, A. F. Hebard, et al., *Science*, **305**, 1273 (2004).
48. M. E. Itkis, S. Niyogi, M. E. Meng, M. A. Hamon, H. Hu, and R. C. Haddon, *Nano Lett.*, **2**, 155 (2002).
49. S. Ji, T. Jiang, K. Xu, and S. Li, *Appl. Surf. Sci.*, **133**, 231 (1998).
50. M. S. Strano, C. A. Dyke, M. L. Usrey, P. W. Barone, M. J. Allen, H. Shan, C. Kittrell, R. H. Hauge, J. M. Tour, and R. E. Smalley, *Science*, **301**, 1519 (2003).
51. R. B. Weisman and S. M. Bachilo, *Nano Lett.*, **3**, 1235 (2003).
52. B. J. Landi, H. J. Ruf, C. M. Evans, C. D. Cress, and R. P. Raffaelle, *J. Phys. Chem. B*, **109**, 9952 (2005).
53. M. S. Jeong, C. C. Byeon, O. H. Cha, H. Jeong, J. H. Han, Y. C. Choi, K. H. An, K. H. Oh, K. K. Kim, and Y. H. Lee, *NANO*, **3**, 101 (2008).
54. Y. Maeda, Y. Takano, A. Sagara, M. Hashimoto, M. Kanda, S. Kimura, Y. Lian, T. Nakahodo, T. Tsuchiya, T. Wakahara, et al., *Carbon*, **46**, 1563 (2008).
55. T. G. Hedderman, A. S. Mostaert, A. E. Shanahan, and H. J. Byrne, *New Carbon Mater.*, **24**, 73 (2009).
56. T. J. McDonald, J. L. Blackburn, W. K. Metzger, G. Rumbles, and M. J. Heben, *J. Phys. Chem. C*, **111**, 17894 (2007).
57. X. Huang, R. S. Mclean, and M. Zheng, *Anal. Chem.*, **77**, 6225 (2005).
58. K. Kamaras, M. E. Itkis, H. Hu, B. Zhao, and R. C. Haddon, *Science*, **301**, 1501 (2003).
59. M. J. Kamlet, H. E. Ungnade, J. P. Phillips, D. Bates, H. Feuer, and B. S. Thyagarajan, in *Organic Electronic Spectral Data*, Wiley Interscience, New York (1989).
60. A. Arrais, R. Gobetto, R. Rossetti, and E. Diana, *New Diamond Front. Carbon Technol.*, **16**, 79 (2006).
61. C. Wang, G. Zhou, J. Wu, B. Gu, and W. Duan, *Appl. Phys. Lett.*, **89**, 173130 (2006).
62. Á. Pekker, D. Wunderlich, K. Kamarás, and A. Hirsch, *Phys. Status Solidi B*, **245**, 1954 (2008).
63. H. Geng, D. S. Lee, K. K. Kim, G. H. Han, H. K. Park, and Y. H. Lee, *Chem. Phys. Lett.*, **455**, 275 (2008).
64. M. Shim and G. P. Siddons, *Appl. Phys. Lett.*, **83**, 3564 (2003).
65. T. Takenobu, Y. Murayama, M. Shiraishi, and Y. Iwasa, *Jpn. J. Appl. Phys., Part 2*, **45**, L1190 (2006).
66. R. A. Jishi, L. Venkataraman, M. S. Dresselhaus, and G. Dresselhaus, *Chem. Phys. Lett.*, **209**, 77 (1993).
67. S. Bandow, S. Asaka, Y. Saito, A. M. Rao, L. Grigorian, E. Richter, and P. C. Eklund, *Phys. Rev. Lett.*, **80**, 3779 (1998).
68. J. Kürti, G. Kresse, and H. Kuzmany, *Phys. Rev. B*, **58**, R8869 (1998).
69. D. Sánchez-Portal, E. Artacho, J. M. Soler, A. Rubio, and P. Ordejón, *Phys. Rev. B*, **59**, 12678 (1999).
70. A. Jorio, R. Saito, J. H. Hafner, C. M. Lieber, M. Hunter, T. McClure, G. Dresselhaus, and M. S. Dresselhaus, *Phys. Rev. Lett.*, **86**, 1118 (2001).
71. T. Chang, *Acta Mech. Sin.*, **23**, 159 (2007).
72. I. L. Li, G. D. Li, H. J. Liu, C. T. Chan, and Z. K. Tang, *Appl. Phys. Lett.*, **82**, 1467 (2003).
73. H. M. Lawler, D. Areshkin, J. W. Mintmire, and C. T. White, *Phys. Rev. B*, **72**, 233403 (2005).
74. V. N. Popov and P. Lambin, *Phys. Rev. B*, **73**, 085407 (2006).
75. M. Hulman, W. Plank, and H. Kuzmany, *Phys. Rev. B*, **63**, 081406(R) (2001).
76. I. O. Maciel, J. Campos-Delgado, E. Cruz-Silva, M. A. Pimenta, B. G. Sumpter, V. Meunier, F. López-Urías, E. Muñoz-Sandoval, H. Terrones, and M. Terrones, *Nano Lett.*, **9**, 2267 (2009).
77. P. T. Araujo, I. O. Maciel, P. B. C. Pesce, M. A. Pimenta, S. K. Doorn, H. Qian, A. Hartschuh, M. Steiner, L. Grigorian, K. Hata, et al., *Phys. Rev. B*, **77**, 241403(R) (2008).
78. J. Tarábek, L. Kavan, L. Dunsch, and M. Kalbac, *J. Phys. Chem. C*, **112**, 13856 (2008).
79. L. Kavan, M. Kalbáč, M. Zukalova, and L. Dunsch, *J. Phys. Chem. B*, **109**, 19613 (2005).
80. M. Burghard, *Surf. Sci. Rep.*, **58**, 1 (2005).
81. S. C. Sharma, D. Singh, and Y. Li, *J. Raman Spectrosc.*, **36**, 755 (2005).
82. R. Graupner, *J. Raman Spectrosc.*, **38**, 673 (2007).
83. A. M. Rao, P. C. Eklund, S. Bandow, A. Thess, and R. E. Smalley, *Nature (London)*, **388**, 257 (1997).